

# First-principles studies of the mixed-dimensional van der Waals heterostructures of graphene/MnF<sub>4</sub>

Cite as: J. Appl. Phys. **132**, 084301 (2022); <https://doi.org/10.1063/5.0101618>

Submitted: 27 June 2022 • Accepted: 30 July 2022 • Published Online: 25 August 2022

 Baojuan Xin,  Kaixin Zou, Dayong Liu, et al.



View Online



Export Citation



CrossMark

## ARTICLES YOU MAY BE INTERESTED IN

Transition metal decorated VSe<sub>2</sub> as promising catechol sensor: Insights from DFT simulations


Journal of Applied Physics **132**, 084502 (2022); <https://doi.org/10.1063/5.0097059>


Field-free current-induced magnetization switching in GdFeCo: A competition between spin-orbit torques and Oersted fields

Journal of Applied Physics **132**, 083903 (2022); <https://doi.org/10.1063/5.0091944>

Straining of atomically thin WSe<sub>2</sub> crystals: Suppressing slippage by thermal annealing

Journal of Applied Physics **132**, 085104 (2022); <https://doi.org/10.1063/5.0096190>






## Instruments for Advanced Science

- Knowledge,
- Experience,
- Expertise


Click to view our product catalogue

Contact Hiden Analytical for further details:  
[www.HidenAnalytical.com](http://www.HidenAnalytical.com)  
[info@hideninc.com](mailto:info@hideninc.com)




Gas Analysis

- ▶ dynamic measurement of reaction gas streams
- ▶ catalysis and thermal analysis
- ▶ molecular beam studies
- ▶ dissolved species probes
- ▶ fermentation, environmental and ecological studies




Surface Science

- ▶ UHVTPD
- ▶ SIMS
- ▶ end point detection in ion beam etch
- ▶ elemental imaging - surface mapping



Plasma Diagnostics

- ▶ plasma source characterization
- ▶ etch and deposition process reaction kinetic studies
- ▶ analysis of neutral and radical species



Vacuum Analysis

- ▶ partial pressure measurement and control of process gases
- ▶ reactive sputter process control
- ▶ vacuum diagnostics
- ▶ vacuum coating process monitoring

# First-principles studies of the mixed-dimensional van der Waals heterostructures of graphene/MnF<sub>4</sub>

Cite as: J. Appl. Phys. 132, 084301 (2022); doi: 10.1063/5.0101618

Submitted: 27 June 2022 · Accepted: 30 July 2022 ·

Published Online: 25 August 2022



View Online



Export Citation



CrossMark

Baojuan Xin,<sup>1</sup> Kaixin Zou,<sup>1</sup> Dayong Liu,<sup>2</sup> Shanchuan Liang,<sup>3</sup> Hong Dong,<sup>1</sup> Feng Lu,<sup>1</sup> Cheng Gong,<sup>3</sup> Feng Luo,<sup>4</sup> and Wei-Hua Wang<sup>1,a)</sup>

## AFFILIATIONS

<sup>1</sup>Department of Electronic Science and Engineering, and Tianjin Key Laboratory of Photo-Electronic Thin Film Device and Technology, Nankai University, Tianjin 300350, China

<sup>2</sup>Department of Physics, School of Sciences, Nantong University, Nantong 226019, China

<sup>3</sup>Department of Electrical and Computer Engineering and Quantum Technology Center, University of Maryland, College Park, Maryland 20742, USA

<sup>4</sup>Department of Materials Science and Engineering, Nankai University, Tianjin 300350, China

<sup>a)</sup>Author to whom correspondence should be addressed: [whwangnk@nankai.edu.cn](mailto:whwangnk@nankai.edu.cn)

## ABSTRACT

Constructing a mixed-dimensional (MD) graphene-based van der Waals heterostructure (vdWH) is a viable technique for opening the bandgap and introducing spin polarization in graphene. In this work, we discovered that the adjacent MnF<sub>4</sub> can manipulate the carrier doping, bandgap opening, and spin polarization of graphene in the MD vdWH of graphene/MnF<sub>4</sub> comprised of two-dimensional (2D) graphene and one-dimensional atomic wire (1D AW) MnF<sub>4</sub>. By adopting first-principles calculations, we found that graphene can achieve effective *p*-type doping with the carrier density up to  $\sim 8.89 \times 10^{13} - 1.03 \times 10^{14} \text{ cm}^{-2}$ . With a twisted angle of  $\theta = 10.89^\circ$  and the compressed distance of  $d_{\text{Mn-Gra}} = 2.84 \text{ \AA}$ , the opened bandgap of graphene ( $E_{\text{g-Gra}}$ ) achieves 35 and 57 meV for spin-up and spin-down channels due to the sublattice symmetry-breaking in graphene, and the spin splitting energy ( $\Delta E_{\text{S}}$ ) at the Dirac point reaches 78.7 meV as a result of the graphene-MnF<sub>4</sub> interlayer interaction. Remarkably,  $E_{\text{g-Gra}}$  is increased to 64 and 79 meV for spin-up and spin-down channels, and  $\Delta E_{\text{S}}$  with 202.7 meV is obtained at  $d_{\text{Mn-Gra}} = 2.84 \text{ \AA}$  when the width of 1D MnF<sub>4</sub> is doubled. Meanwhile, the *n*-type Ohmic contact is also realized. Our work underscores the rich interplay in the graphene/MnF<sub>4</sub> MD vdWH and provides a significant route with fundamental insights to engineer the spintronic band properties of graphene.

Published under an exclusive license by AIP Publishing. <https://doi.org/10.1063/5.0101618>

## I. INTRODUCTION

Graphene is promising to be applied in spin field-effect transistor (FET) devices with high-speed and low-power consumption due to its superior electrical properties and long spin-diffusion lengths.<sup>1-3</sup> Nevertheless, along with its low carrier density, zero bandgap, and weak spin-orbit coupling, pristine graphene's electrical conductivity as electrodes, direct operation as channels, and applicability in spin-relevant devices are limited.<sup>4-7</sup> Although the introduced dopants, defects, edge states of nanoribbons, or external electric field, etc., could achieve carrier doping, open the bandgap or realize spin polarization of graphene and other two-dimensional (2D) materials,<sup>8-17</sup> the inducing disorders or dopant scattering centers would suppress the carrier mobility. Thus, it is significant

to explore the strategies for achieving effective carrier doping, the bandgap opening, and the spin polarization in graphene under the premise of maintaining its superior carrier transport properties.

Constructing van der Waals heterostructures (vdWHs) through stacking different 2D monolayers with graphene is one of the effective schemes to engineer the electronic structures of graphene.<sup>18-30</sup> For example, the bandgap of graphene with few tens of meV has been achieved in vdWHs of graphene/WSe<sub>2</sub>, graphene/C<sub>3</sub>N, graphene/MXene, etc.<sup>18-24</sup> Besides, stacking magnetic materials on graphene is one convenient and possible strategy to introduce the spin polarization via the magnetic proximity effect, such as in graphene/CrI<sub>3</sub>, graphene/CrBr<sub>3</sub>, etc.<sup>25-30</sup> Significantly, the high carrier mobility is almost reserved since the

weak interlayer coupling within the vdWH does not impact the electronic properties of graphene near the Dirac point.

In addition to 2D materials, one-dimensional (1D) systems such as carbon nanotubes and 1D atom wires (AWs) have been reported.<sup>31–33</sup> Especially, our previous reports have predicted many kinds of 1D AWs with atomic scale widths.<sup>34</sup> These 1D AWs could be constructed in the mixed-dimensional (MD) vdWHs with graphene.<sup>35</sup> The MD vdWHs possess various stacking configurations compared with 2D/2D vdWHs, providing more possibilities to further manipulate the structures and electronic structures of graphene and other low-dimensional materials.<sup>36–40</sup> Therefore, the MD vdWHs would expand the platform and offer more opportunities to further manipulate the exotic electronic states of low-dimensional systems.

In this work, 1D ferromagnetic (FM) semiconductor  $\text{MnF}_4$  was selected to construct graphene-based MD vdWH of graphene/ $\text{MnF}_4$  because it would be expected to introduce spin polarization into graphene by the magnetic proximity effect through various stacking configurations. The carrier doping, electronic structure, and spin polarization of graphene/ $\text{MnF}_4$  have been systematically investigated by first-principles calculations. The most stable MD vdWH structure was obtained by translating and revolving  $\text{MnF}_4$  relative to graphene. The electronic states and spin polarization of graphene could be manipulated by modulating the distance, twisting angle between  $\text{MnF}_4$  and graphene, or the width of the 1D AW  $\text{MnF}_4$ . Also, the contact between graphene and  $\text{MnF}_4$  within the MD vdWH has been analyzed to provide more fundamental guidance for further practical spintronic and optoelectronic devices.

## II. COMPUTATIONAL METHODS

The geometrical and electronic structures of  $\text{MnF}_4$  and the MD vdWH of graphene/ $\text{MnF}_4$  have been investigated by using the Vienna *ab initio* simulation package (VASP) code.<sup>41</sup> The exchange-correlation potential was described by the generalized gradient approximation with the Perdew–Burke–Ernzerhof (GGA-PBE) functional.<sup>42</sup> The cutoff energy was set as 500 eV in all calculations. The *k*-point grids of  $15 \times 1 \times 1$  and  $5 \times 5 \times 1$  were adopted for  $\text{MnF}_4$  and the vdWH supercell of graphene/ $\text{MnF}_4$ , respectively. The structure relaxation stopped until the force was less than  $0.02 \text{ eV } \text{\AA}^{-1}$  per atom, and the energy convergence criterion was set to be  $10^{-4} \text{ eV}$ . The Grimme's zero damping DFT-D2 method was considered here.<sup>43</sup> To avoid the interactions between two adjacent vertical layers, a vacuum with a thickness of 20 Å was adopted.

## III. RESULTS AND DISCUSSIONS

### A. Geometrical structure, stability, and electronic structures of 1D AW $\text{MnF}_4$

As shown in Fig. 1(a), the relaxed lattice constant, the Mn–F–Mn bond angle ( $\beta$ ), and the nearest Mn–Mn distance ( $d$ ) of the 1D AW  $\text{MnF}_4$  are 5.91 Å,  $\sim 101.1^\circ$ , and 2.95 Å, respectively, which are consistent with the reported data.<sup>34</sup> 1D  $\text{MnF}_4$  is also thermodynamically stable due to the absence of the imaginary frequency in the phonon spectra in Fig. 1(d). Through comparing different magnetic configurations, the FM state is energetically stable and 1D  $\text{MnF}_4$  demonstrates a FM semiconductor with the bandgap

of 0.36 eV in Fig. 1(e), where the magnetic moment of Mn is  $\sim 2.65 \mu_B$ . Although Mn- $d_{xy}$ ,  $d_{xz}$ , and  $d_{yz}$  orbitals in 1D AW  $\text{MnF}_4$  are nearly half-filled in a distorted octahedral crystal field, the splitting energy between the highest level in  $t_{2g}$  groups and the lowest level in  $e_g$  groups is relatively small, as presented in Fig. S1 of the supplementary material. Moreover, even if the Hubbard  $U = 4 \text{ eV}$  is considered in 1D  $\text{MnF}_4$ , the FM state is still energetically stable due to the small splitting energy under the distorted octahedral crystal field. Thus, the FM state in 1D  $\text{MnF}_4$  is more energetically stable than the antiferromagnetic state, which is different from the antiferromagnetic state in 2D  $\text{MnF}_4$ .<sup>44</sup>

### B. Geometrical structure, stability, and electronic structures of MD vdWH graphene/ $\text{MnF}_4$

The side and top views of the MD vdWH are shown in Figs. 1(b) and 1(c). To minimize the lattice mismatch and the interactions within the periodical 1D AWs in the 2D plane, the large MD vdWH supercell is constructed with  $4 \times 1 \times 1 \text{ MnF}_4$  and  $5 \times 3\sqrt{3} \times 1$  graphene. The lattice parameters are set based on graphene and the lattice mismatch for  $\text{MnF}_4$  is  $\sim 3.99\%$ . Through exploring the possible stacking configurations between graphene and  $\text{MnF}_4$  shown in Fig. S2 in the supplementary material, the most favorable stacking structure is selected and analyzed. For the stable MD vdWH, the  $d_{\text{Mn-Gra}}$  between Mn atoms and graphene is 3.84 Å, and the formation energy is  $-0.093 \text{ eV/atom}$ . Moreover, the energetically favorable magnetic configuration of  $\text{MnF}_4$  is still FM within the MD vdWH.

The fundamental electronic structures of MD vdWH are shown in Fig. 2. The Fermi level ( $E_F$ ) is shifted downward away from the Dirac point of  $\sim 0.95 \text{ eV}$ , demonstrating the effective *p*-type doping of graphene. Combined with the Bader charge analysis,<sup>45</sup>  $\sim 1.40 e$  transfers from graphene to  $\text{MnF}_4$  in the supercell, thereby resulting in the *p*-type carrier density of  $8.89 \times 10^{13} \text{ cm}^{-2}$  for graphene in Table I. Compared with other graphene-based vdWHs, graphene transfers more electrons to  $\text{MnF}_4$  due to the stronger electronegativity of F atoms than C atoms. It is found that a bandgap of 15 meV is opened for the spin-up channel of graphene at the Dirac point and the metallic character remains for the spin-down channel in Fig. 2(a).

Enhancing the interlayer interaction through compressing the equilibrium distance is an effective way to tune the electronic states of graphene in the vdWH. As listed in Table I, it is still stable at the compressed distance of  $d_{\text{Mn-Gra}} = 2.84 \text{ \AA}$  for most the cases. In addition, the theoretically vertical pressure is estimated as  $\sim 6.10 \text{ GPa}$  when the distance between graphene and  $\text{MnF}_4$  ( $d_{\text{Mn-Gra}}$ ) was compressed to 2.84 from 3.84 Å through the formula of  $p(d) = \Delta E / (S \cdot |\Delta d|)$ , where  $\Delta E$ ,  $S$ , and  $\Delta d$  are the energy difference between the compressed and the equilibrium heterostructures, the area of the interface, and the distance change, respectively.<sup>25</sup> The vertical pressure of  $\sim 6.10 \text{ GPa}$  in vdWH graphene/ $\text{MnF}_4$  is feasible in experiments, since the experimental pressure of 30–50 GPa could be realized in graphite,  $\text{MoS}_2$ , and other 2D materials with the quantum phase transition or the metastable phase appearance.<sup>46–48</sup> Moreover, the vertical pressure is less than that in the compressed vdWH of graphene/ $\text{CrI}_3$ .<sup>25</sup>

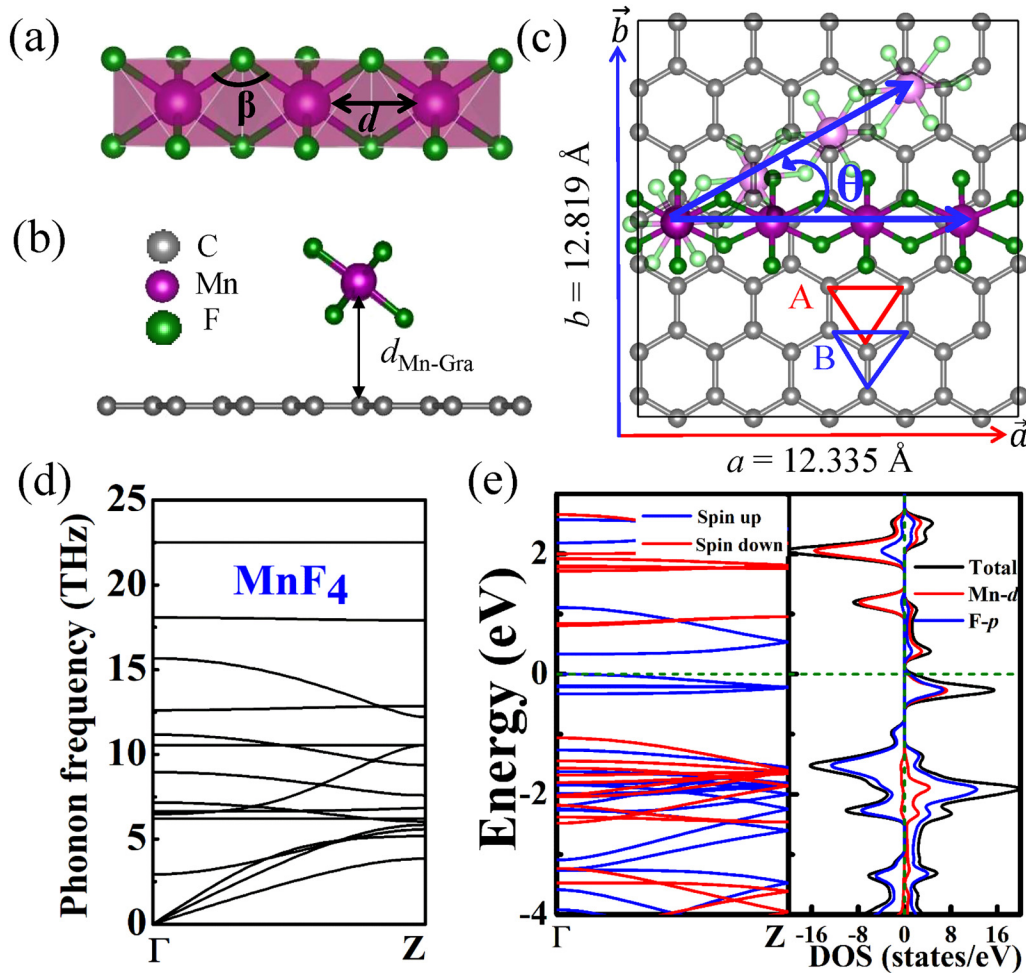


**FIG. 1.** (a) Top view of 1D AW  $\text{MnF}_4$ ,  $\beta$ , and  $d$  are the Mn–F–Mn bond angle and the nearest Mn–Mn distance, respectively. (b) Side and (c) top views of vdWH graphene/ $\text{MnF}_4$ .  $d_{\text{Mn-Gra}}$  and  $\theta$  are defined as the vdW distance and the anticlockwise twisting angle between the Mn atoms and graphene plane. The rectangle outlined by black lines is the supercell of the vdWH. A and B represent two types of sublattices in graphene. Gray, purple, and olive spheres represent C atoms, Mn atoms, and F atoms, respectively. The twisted  $\text{MnF}_4$  is displayed by light purple and light olive spheres relative to the pristine stacking one. (d) Phonon spectra of  $\text{MnF}_4$  along the high symmetric direction in the reduced Brillouin zone. (e) Band structure and density of states (DOS) of  $\text{MnF}_4$ .

According to the Bader charge analysis,<sup>45</sup> the inequivalent electron transfer from two types of C atoms ( $C_A$  and  $C_B$ ) to  $\text{MnF}_4$  breaks the sublattice symmetry of graphene. As shown in Fig. 1(c), the mean distance from  $C_A$  atoms to the nearest Mn atoms is closer than that of  $C_B$  atoms under  $d_{\text{Mn-Gra}} = 3.84 \text{ \AA}$ , leading to  $0.34 e$  more charge transfer of  $C_A$  atoms than  $C_B$  atoms. At  $d_{\text{Mn-Gra}} = 2.84 \text{ \AA}$ , the charge transfer difference of  $0.78 e$  occurs between  $C_A$  atoms and  $C_B$  atoms. Due to the slightly different electrostatic potential modulation on the sublattice of graphene, the bandgap of graphene ( $E_{\text{g-Gra}}$ ) is opened. As shown in Fig. 2(b),  $E_{\text{g-Gra}}$  is  $\sim 22$  and  $\sim 4 \text{ meV}$  for spin-up and spin-down channels, respectively. Besides, the different contribution of  $C_A$  and  $C_B$  atoms in spin-up and spin-down states leads to the spin splitting of graphene around the Dirac point.

The spin polarization of graphene could be realized through the interaction between graphene and  $\text{MnF}_4$ . Compared to the regular octahedral ( $O_h$ ) crystal field in Fig. 3(a), the FM semiconductor of  $\text{MnF}_4$  possesses the distorted  $O_h$  crystal field in Fig. 3(b). As displayed in Fig. 3(b), on the basis of  $3d$ -orbitals splitting under a regular  $O_h$  crystal field, the  $e_g$  group further splits into  $d_{x^2-y^2}$  and  $d_{3z^2-r^2}$  and  $t_{2g}$  group splits into  $d_{xy}$  and  $d_{xz}, d_{yz}$  under distorted  $O_h$  crystal field. For 1D  $\text{MnF}_4$ , the Mn- $3d$  electrons in the  $\text{Mn}^{4+}$  state would occupy the spin-up states in  $d_{xy}, d_{xz}$ , and  $d_{yz}$  orbitals. Compared with the pristine  $\text{MnF}_4$ , the relative locations between Mn atoms of  $\text{MnF}_4$  and C atoms of graphene are different in MD vdWH. Thus, the magnetic moments of Mn atoms in  $\text{MnF}_4$  are divided into two groups, where Mn-I and Mn-II are defined with relatively larger and smaller magnetic moments, respectively. For  $\theta = 0.0^\circ$ , the mean magnetic moments of

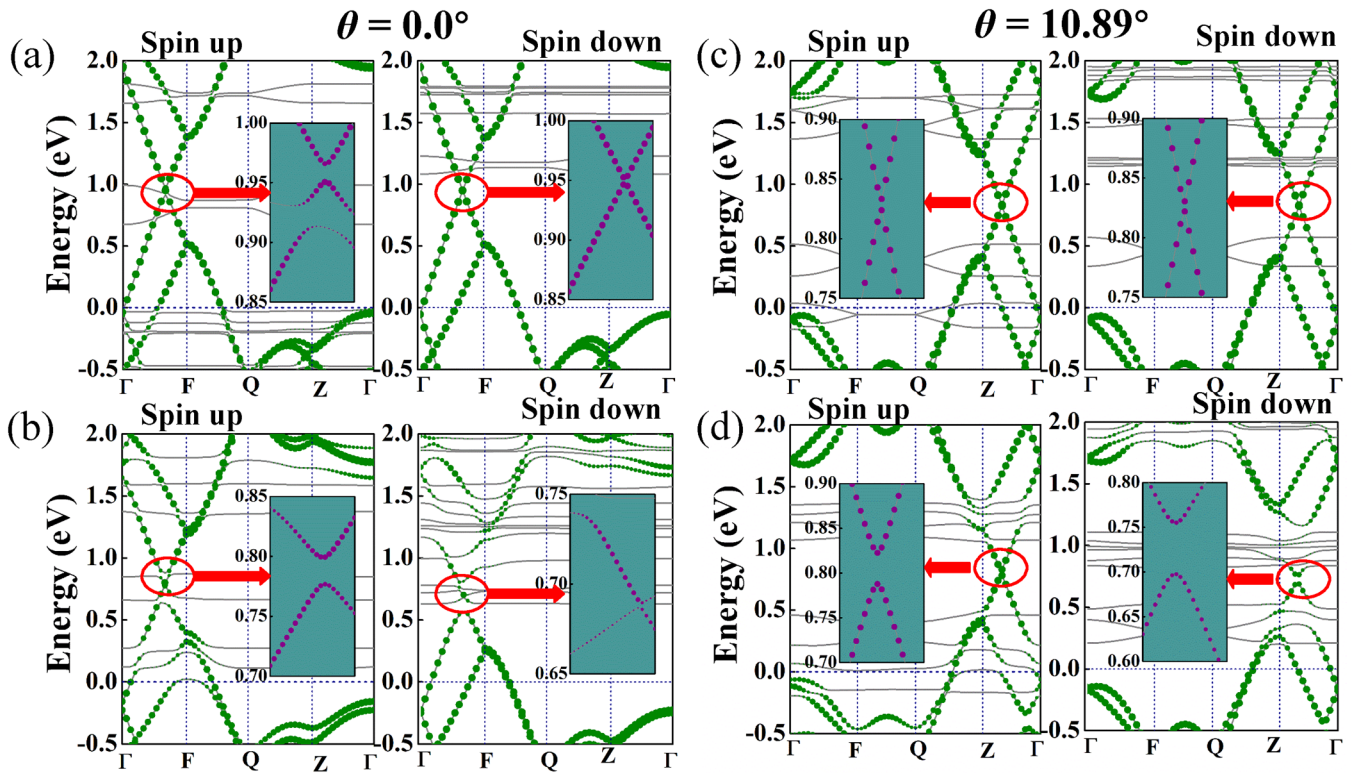
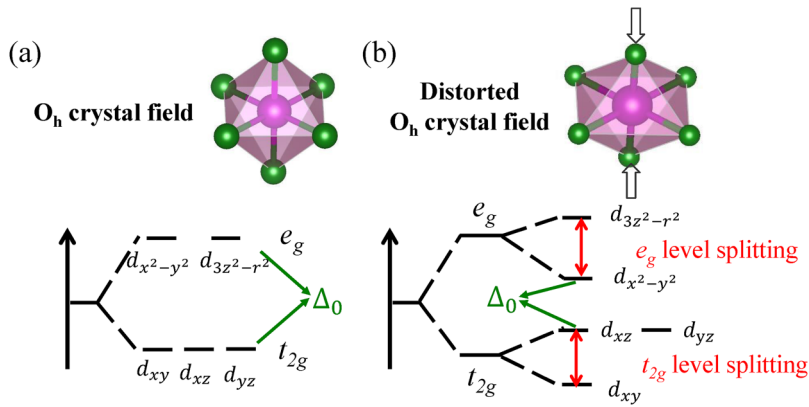


FIG. 2. At pristine stacking configuration with  $\theta = 0.0^\circ$ , the band structures of graphene/ $\text{MnF}_4$  at the equilibrium distance  $d_{\text{Mn-Gra}} = 3.84 \text{ \AA}$  in (a) and at the compressed  $d_{\text{Mn-Gra}} = 2.84 \text{ \AA}$  in (b). The olive dots display the contribution of graphene. Insets show the zoom-in electronic states within the regime of the red circles, where the purple dots represent the contribution of graphene. (c) and (d) correspond to  $\theta = 10.89^\circ$  but  $d_{\text{Mn-Gra}} = 3.98 \text{ \AA}$  in (c) and  $d_{\text{Mn-Gra}} = 2.84 \text{ \AA}$  in (d).

TABLE I. The formation energy of vdWH ( $E_{\text{form}}$ ) with  $E_{\text{form}} = (E_{\text{vdWH}} - E_{\text{graphene}} - E_{\text{MnF}_4})/N$  (here  $E_{\text{form}}$ ,  $E_{\text{graphene}}$  and  $E_{\text{MnF}_4}$  represent the total energies of vdWH, graphene, and  $\text{MnF}_4$ , respectively, and  $N$  is the number of atoms in the vdWH supercell), the carrier density of graphene ( $\rho_{\text{Gra}}$ ), the magnetic moments of  $M_{\text{Mn-I}}$  and  $M_{\text{Mn-II}}$ , the spin splitting energy of vdWH ( $\Delta E_S$ ), the bandgaps of graphene ( $E_{\text{g-Gra}}$ ) for spin-up ( $\uparrow$ ) and spin-down ( $\downarrow$ ) channels within the vdWH supercell at different distance  $d_{\text{Mn-Gra}}$  under different twisting angles.

$\theta$	$d_{\text{Mn-Gra}}$ ( $\text{\AA}$ )	$E_{\text{form}}$ (eV/atom)	$\rho_{\text{Gra}}$ ( $\times 10^{13} \text{ cm}^{-2}$ )	$M_{\text{Mn-I}}$ ( $\mu_B$ )	$M_{\text{Mn-II}}$ ( $\mu_B$ )	$\Delta E_S$ (meV)	$E_{\text{g-Gra}}$ (meV)	
							$\uparrow$	$\downarrow$
$0.0^\circ$	3.84	-0.093	8.89	3.325	2.751	8.8	15	0
	2.84	-0.018	7.55	3.537	2.678	99.9	22	4
$10.89^\circ$	3.98	-0.087	7.83	3.201	2.676	2.5	0	0
	2.84	0.007	8.15	3.511	2.702	78.7	35	57
$13.90^\circ$	3.98	-0.089	6.48	2.778	2.185	1.6	0	0
	2.84	-0.016	7.26	3.478	2.715	32.3	28	51
$30.00^\circ$	4.15	-0.086	6.62	3.514	2.724	0	0	0
	2.84	-0.002	7.45	3.505	2.654	75.8	6	38
$46.10^\circ$	3.98	-0.089	7.11	3.580	2.693	2.4	0	0
	2.84	-0.017	7.36	3.485	2.712	22.9	18	50
$49.11^\circ$	4.09	-0.086	7.66	3.186	2.679	2.0	0	0
	2.84	0.008	8.35	3.164	2.689	102.1	41	19



**FIG. 3.** Schematic diagrams of regular and distorted octahedral crystal fields in (a) and (b), and the corresponding Mn-3d orbitals splitting.  $\Delta_0$  represents the splitting energy between the highest level in  $t_{2g}$  groups and the lowest level in  $e_g$  groups.

Mn-I and Mn-II in Table I are increased relative to the pristine 1D  $\text{MnF}_4$ , which are induced by two factors. On one hand, the  $O_h$  crystal field distortion gets greater within the MD vdWH, thereby resulting in the decreased energy difference  $\Delta_0$ . The competition between Hund's coupling and  $\Delta_0$  results in a larger magnetic moment of Mn in the MD vdWH. On the other hand, the spin-up electrons in graphene prefer to transfer to  $\text{MnF}_4$  and occupy the spin-up  $d_{x^2-y^2}$  orbital and  $d_{xz}$ ,  $d_{yz}$  orbitals for Mn-I and Mn-II ions, respectively, leading to the increase of the magnetic moments of Mn ions and the more stable FM ground state in the MD vdWH. More significantly, the spin

polarization of graphene is triggered. The spin splitting energy ( $\Delta E_s$ ) is 8.8 meV at  $d_{\text{Mn-Gra}} = 3.84 \text{ \AA}$  and it is improved to 99.9 meV at  $d_{\text{Mn-Gra}} = 2.84 \text{ \AA}$ , which is induced by the different contributions of  $C_A$  atoms and  $C_B$  atoms in spin-up and spin-down states. As shown in the partial density of states (PDOS) of graphene, the contributions from  $C_A$  and  $C_B$  sublattice are slightly different for spin-up and spin-down states at  $d_{\text{Mn-Gra}} = 3.84 \text{ \AA}$  in Fig. 4(a), and the obvious contribution difference of  $C_A$  and  $C_B$  atoms is presented at  $d_{\text{Mn-Gra}} = 2.84 \text{ \AA}$  in Fig. 4(b). Thus,  $\Delta E_s$  is increased to  $\sim 99.9 \text{ meV}$  in Fig. 4(b) relative to 8.8 meV in Fig. 4(a).

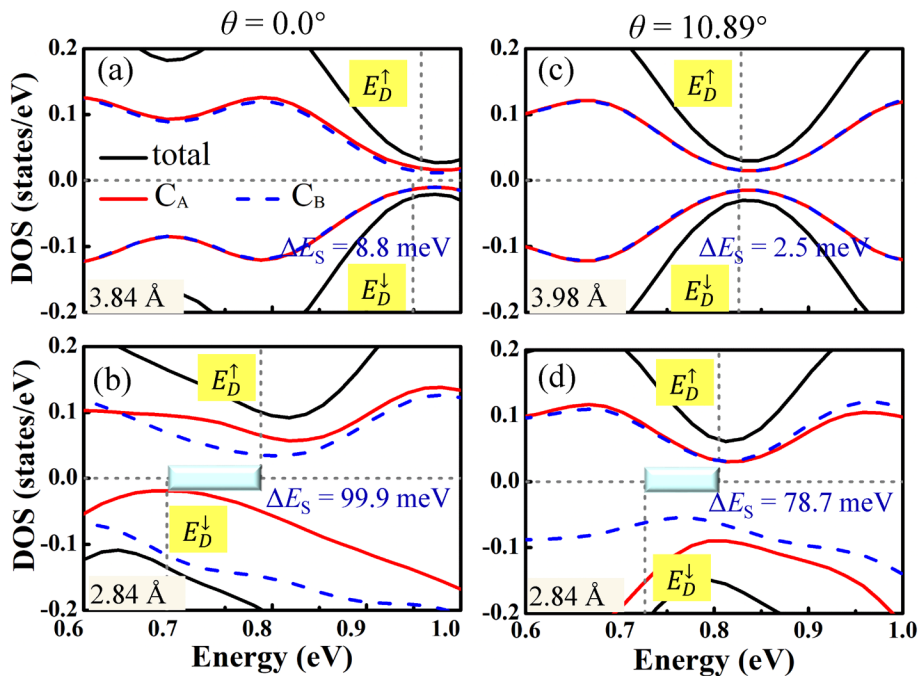


**FIG. 4.** The spin-resolved partial density of states (PDOS) for sublattice  $C_A$  and  $C_B$  of graphene near the Dirac point. (a)  $\theta = 0.0^\circ$  and  $d_{\text{Mn-Gra}} = 3.84 \text{ \AA}$ , (b)  $\theta = 0.0^\circ$  and  $d_{\text{Mn-Gra}} = 2.84 \text{ \AA}$ , (c)  $\theta = 10.89^\circ$  and  $d_{\text{Mn-Gra}} = 3.98 \text{ \AA}$ , (d)  $\theta = 10.89^\circ$  and  $d_{\text{Mn-Gra}} = 2.84 \text{ \AA}$ .  $E_D^\uparrow$  and  $E_D^\downarrow$  represent the energies of the Dirac point for the spin-up and spin-down channels, respectively.  $\Delta E_s$  is the spin splitting energy.

### C. Effect of twisting angle on stability and electronic structures of MD vdWH graphene/MnF<sub>4</sub>

The exotic quantum states would appear in twisted bilayer graphene and other vdWHs because of the variation of periodic potential and interlayer coupling interaction. For instance, the flatbands take place in magic-angle bilayer graphene and in twisted bilayer GeSe, etc.<sup>49–52</sup> Thus, the modulation of electronic structures and spin polarization of graphene are expected within twisted MD vdWH of graphene/MnF<sub>4</sub> as the twisting angle changes. In this work,  $\theta = 10.89^\circ, 13.90^\circ, 30.00^\circ, 46.10^\circ,$  and  $49.11^\circ$  are considered. As listed in Table I, the equilibrium distance is slightly enlarged to 3.98 Å for  $\theta = 10.89^\circ$  case, which results from the steric effects.<sup>53</sup> In detail, the F atoms of MnF<sub>4</sub> are almost located above the hexagonal hollow positions of C atoms under the most energetically favorable stacking configuration at  $\theta = 0.0^\circ$  in Fig. S2(i) in the [supplementary material](#). In contrast, the F atoms are mostly directly located on the top of C atoms in the energetically unfavorable state, which induces strong repulsion interaction, as shown in Fig. S2(h) in the [supplementary material](#). At other twisting angles in Table I, the interlayer repulsion is regarded as within the range of the most

unstable and stable stacking configurations. Therefore, the equilibrium interlayer distance would increase in twisted vdWHs to weaken the interlayer interaction. It is noted that the case with the same compressed  $d_{\text{Mn-Gra}} = 2.84 \text{ \AA}$  for all twisted vdWHs is explored in this work to examine the enhanced interlayer interaction. Although the slightly positive  $E_{\text{form}}$  with 0.007 eV/atom at  $\theta = 10.89^\circ$  and  $d_{\text{Mn-Gra}} = 2.84 \text{ \AA}$  implies the metastable vdWH of graphene/MnF<sub>4</sub>, it could be achieved with a vertical pressure of  $\sim 6.80 \text{ GPa}$ . Besides, the similar compressed vdWHs with much larger  $E_{\text{form}}$  of 0.15–0.20 eV/atom have been reported in graphene/GeC and graphene/As systems.<sup>54,55</sup>

Under the equilibrium distance of  $d_{\text{Mn-Gra}} = 3.98 \text{ \AA}$ , no bandgap is opened for MD vdWH at  $\theta = 10.89^\circ$  in Fig. 2(c). Similarly, when  $d_{\text{Mn-Gra}}$  is compressed to 2.84 Å, the sublattice symmetry is broken due to the difference of 0.72 e in the charge transfer for C<sub>A</sub> and C<sub>B</sub> atoms. Thus, the opened  $E_{\text{g-Gra}}$  is up to 35 and 57 meV for spin-up and spin-down channels in Fig. 2(d). Remarkably, the linear dispersions of graphene outlined by the red circles and zoomed in the insets in Fig. 2(d) are also well maintained. Moreover, the PDOS contribution difference of C<sub>A</sub> and C<sub>B</sub> sublattice in two spin channels for  $\theta = 10.89^\circ$  is also evident at the

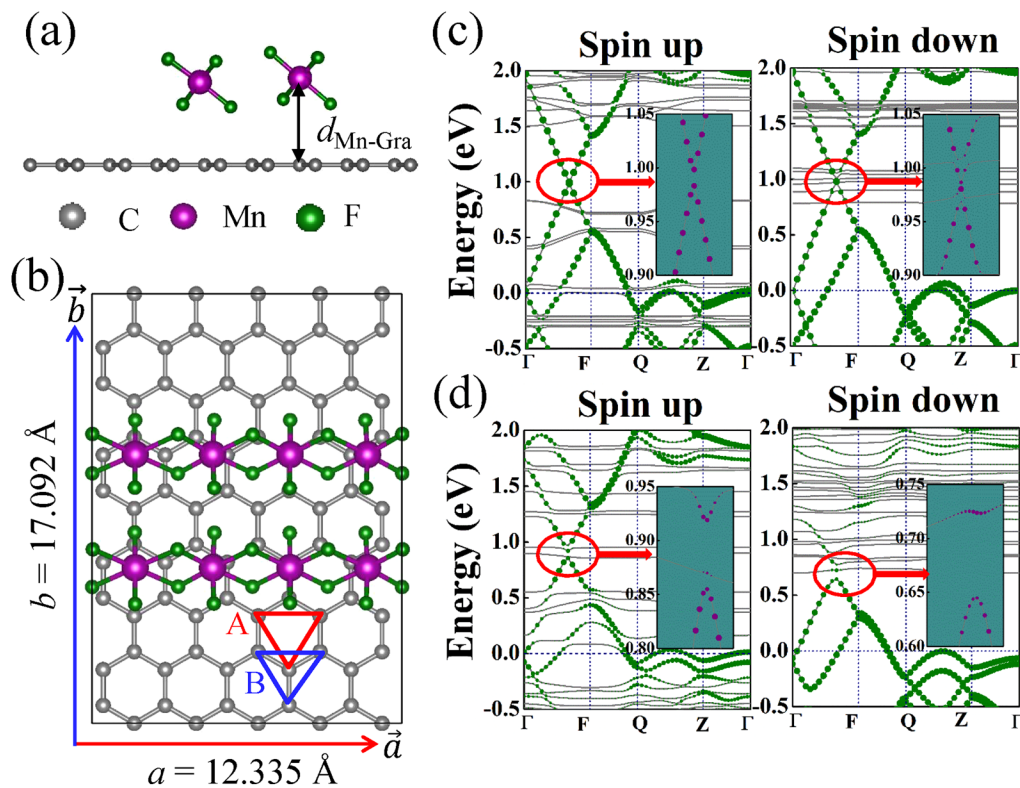


**FIG. 5.** (a) Side and (b) top view of graphene/DC-MnF<sub>4</sub> vdWH.  $d_{\text{Mn-Gra}}$  is defined as the vdW distance between the Mn atoms and graphene plane. The rectangle outlined by black lines is the supercell of graphene/DC-MnF<sub>4</sub> vdWH. A and B represent two types of sublattices in graphene. Gray, purple, and olive spheres represent C atoms, Mn atoms, and F atoms, respectively. The band structures of graphene/DC-MnF<sub>4</sub> vdWH at the equilibrium distance ( $d_{\text{Mn-Gra}} = 3.90 \text{ \AA}$ ) in (c), the compressed  $d_{\text{Mn-Gra}} = 2.84 \text{ \AA}$  in (d). The olive dots display the contribution of graphene. Insets show the zoom-in images within the range of red circles, where the purple dots represent the contribution of graphene.

compressed  $d_{\text{Mn-Gra}} = 2.84 \text{ \AA}$  in Fig. 4(d). Consequently,  $\Delta E_s$  is  $\sim 2.5$  and  $\sim 78.7$  meV in Figs. 4(c) and 4(d), respectively.  $E_{g-\text{Gra}}$  and  $\Delta E_s$  of graphene within the vdWHs at other twisting angles are summarized in Table I, and the detailed band structures are presented in Fig. S3 in the supplementary material. Similar to the case of  $\theta = 10.89^\circ$ ,  $E_{g-\text{Gra}}$  and  $\Delta E_s$  of graphene within vdWHs are ignorable at the equilibrium distance, but they are enhanced at  $d_{\text{Mn-Gra}} = 2.84 \text{ \AA}$ . Meanwhile, to alleviate the concerns on the slightly positive  $E_{\text{form}}$ , the vdWH of graphene/MnF<sub>4</sub> at  $\theta = 10.89^\circ$  and  $d_{\text{Mn-Gra}} = 3.04 \text{ \AA}$  has also been examined and  $E_{\text{form}}$  of  $-0.032$  eV/atom is obtained. The detailed band structures are presented in Fig. S4 in the supplementary material.

#### D. Width effect of 1D MnF<sub>4</sub> on stability and electronic structures of MD vdWH graphene/MnF<sub>4</sub>

In addition to the distance and the twisting angles between graphene and MnF<sub>4</sub>, the width of the 1D AW in MD vdWH would modulate the electronic states of graphene, which is distinguished from the traditional 2D/2D vdWH. To unveil the effect of the width, the 1D MnF<sub>4</sub> is widened to include two closely packed MnF<sub>4</sub> chains same as its bulk structure, which is defined as the DC-MnF<sub>4</sub>. The electronic and magnetic properties of graphene/DC-MnF<sub>4</sub> have been explored. A  $4 \times 1 \times 1$  supercell of DC-MnF<sub>4</sub> and a  $5 \times 4\sqrt{3} \times 1$  supercell of graphene was used to build the MD vdWH, as shown in Figs. 5(a) and 5(b). The relaxed structure indicates that the equilibrium distance is  $d_{\text{Mn-Gra}} = 3.90 \text{ \AA}$  under the most stable configuration with the formation energy of  $-0.044$  eV/atom, where both the intra-chain and the inter-chain within MnF<sub>4</sub> are FM. Figures 5(c) and 5(d) display the band structures of graphene/DC-MnF<sub>4</sub> at the equilibrium distance

$d_{\text{Mn-Gra}} = 3.90 \text{ \AA}$  and the compressed distance  $d_{\text{Mn-Gra}} = 2.84 \text{ \AA}$ . At  $d_{\text{Mn-Gra}} = 3.90 \text{ \AA}$ , it is found that  $E_{g-\text{Gra}}$  is 15 and 0 meV for the spin-up channel and spin-down channel around the Dirac point of graphene, respectively. The opened maximum  $E_{g-\text{Gra}}$  is 64 meV for the spin-up channel and 79 meV for the spin-down channel at  $d_{\text{Mn-Gra}} = 2.84 \text{ \AA}$ . Compared with the above-mentioned graphene/MnF<sub>4</sub> vdWH, the carrier density and  $E_{g-\text{Gra}}$  are both increased with the increased width of MnF<sub>4</sub>, especially, the carrier density is up to  $\sim 1.03 \times 10^{14} \text{ cm}^{-2}$ . The spin polarization of graphene within graphene/DC-MnF<sub>4</sub> vdWH is considerably increased owing to the even greater difference between the contribution of C<sub>A</sub> and C<sub>B</sub> sublattice in Fig. S5 in the supplementary material. As displayed in Fig. S5(b) in the supplementary material, the splitting energy ( $\Delta E_s$ ) of the vdWH is increased to 202.7 meV at  $d_{\text{Mn-Gra}} = 2.84 \text{ \AA}$ , which is considerably improved compared with 2D/2D vdWHs like graphene/CrI<sub>3</sub>, graphene/Cr<sub>2</sub>Ge<sub>2</sub>Te<sub>6</sub>, etc.<sup>25,29</sup>

#### E. Band alignment and contact type for the MD vdWH graphene/MnF<sub>4</sub>

Besides the modulation of graphene in MD vdWH of graphene/MnF<sub>4</sub>, the metal/semiconductor contact interface is also critical for device applications. To explore graphene/MnF<sub>4</sub> interface contact, their schematic energy level diagrams before and after contact are shown in Figs. 6(a) and 6(b). Due to the different work functions of graphene ( $W_{\text{Gra}}$ ) and MnF<sub>4</sub> ( $W_{\text{MnF}_4}$ ), an interface dipole occurs, which is obtained via the potential step. The potential step is inferred to be  $\sim 3.81$  eV in Fig. 6(c). To align  $E_F$  within the MD vdWH,  $E_F$  of MnF<sub>4</sub> would shift upward. With the change of  $E_F$ , the conduction band and the valence band of MnF<sub>4</sub> are both pulled upward. According to the Schottky-Mott

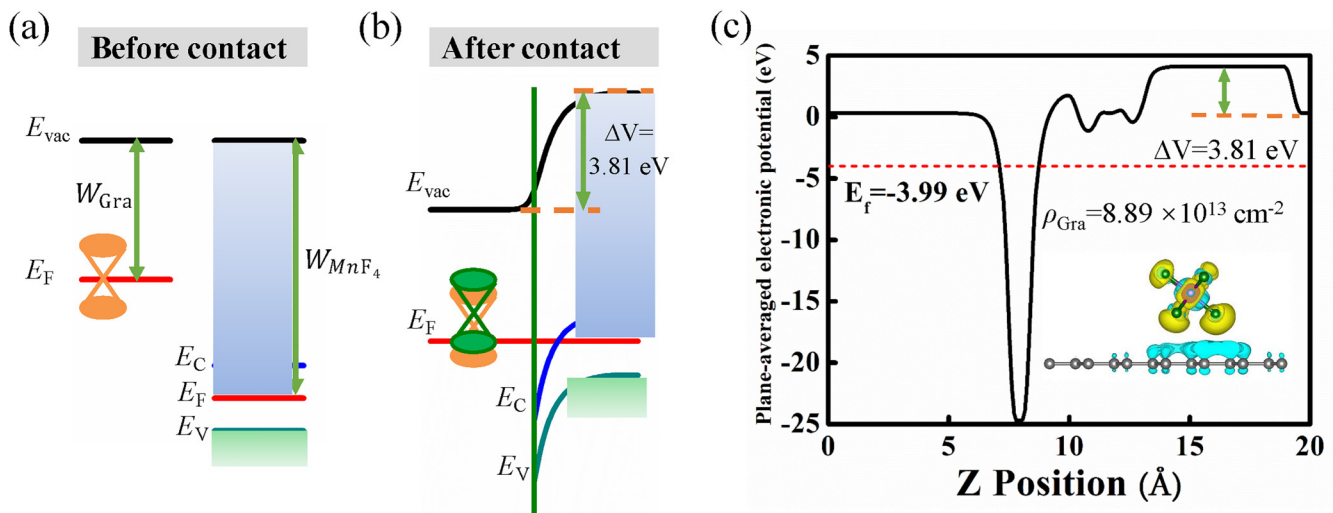


**FIG. 6.** Schematic diagram of energy levels corresponding to graphene and MnF<sub>4</sub> before contact in (a) and after contact at the equilibrium distance in (b).  $W_{\text{Gra}}$ ,  $W_{\text{MnF}_4}$ ,  $E_{\text{vac}}$ , and  $E_F$  represent the work functions of graphene, MnF<sub>4</sub>, the vacuum level, and the Fermi level, respectively.  $\Delta V$  represents the potential step formed at the graphene/MnF<sub>4</sub> interface. (c) The plane-averaged electronic potential along the Z axis for MD vdWH at  $d_{\text{Mn-Gra}} = 3.84 \text{ \AA}$  and  $\theta = 0.0^\circ$ . The corresponding differential charge density of the vdWH is shown in the inset. Yellow and cyan represent the charge accumulation and depletion, respectively, with the iso-surface value of  $0.01 \text{ e/\AA}^3$ .



model,<sup>56</sup> an *n*-type Ohmic contact would form in vdWH owing to the aligned  $E_F$  crossing the conduction band of  $\text{MnF}_4$  in Fig. 6(b). As denoted in the inset of Fig. 6(c), the charge accumulation and depletion occur in  $\text{MnF}_4$  and graphene, respectively. For the MD vdWH of graphene/DC- $\text{MnF}_4$ , more electrons transfer from graphene to  $\text{MnF}_4$  and the potential step increases to  $\sim 4.09$  eV. Additionally, the *n*-type Ohmic contact remained in MD vdWH of graphene/DC- $\text{MnF}_4$ .

The feasibility to experimentally prepare the MD vdWH of graphene/ $\text{MnF}_4$  is expected to be examined by experimental experts. The corresponding bulk materials for graphene and 1D AW of  $\text{MnF}_4$  are both vdW materials, where the interlayer or interwire vdW interaction is weak. Thus, graphene can be exfoliated from graphite in experiments and the cleavage energy is  $\sim 52$  meV/atom.<sup>1,57</sup> The 1D atomic wire of  $\text{MnF}_4$  is expected to be exfoliated from its bulk material owing to its relatively lower cleavage energy of 37 meV/atom compared with that of graphite.<sup>34</sup> Through the mechanical exfoliation method, graphene and 1D  $\text{MnF}_4$  could be feasibly prepared. Furthermore, the proposed vdWH of graphene/ $\text{MnF}_4$  could be constructed by direct stacking similar to other vdWHs,<sup>58,59</sup> which is also highly desirable to be examined in experiments.

#### IV. CONCLUSIONS

In summary, the fundamental electronic structures and magnetic properties of MD vdWH of graphene/ $\text{MnF}_4$  have been investigated based on first-principles calculations. Due to the sublattice symmetry breaking of graphene and the interlayer interaction, the bandgap opening and the spin polarization of graphene have been achieved, which could also be manipulated by modulating the distance of  $d_{\text{Mn-Gr}}$ , the twisting angle  $\theta$ , or the width of 1D  $\text{MnF}_4$ . Significantly, graphene achieves effective *p*-type doping and its carrier density is up to  $10^{14}$   $\text{cm}^{-2}$  due to the charge transfer from graphene to  $\text{MnF}_4$ . Moreover, the *n*-type Ohmic contact is realized in MD vdWH of graphene/ $\text{MnF}_4$ . These theoretical results would provide significant insights for manipulating the electronic structures and spin polarization of graphene and other low-dimensional systems through constructing MD vdWHs.

#### SUPPLEMENTARY MATERIAL

See the [supplementary material](#) for the magnetic properties of  $\text{MnF}_4$ , six different configurations of MD vdWH, electronic structures of vdWHs at different  $d_{\text{Mn-Gr}}$ , different twisting angles, and different widths of  $\text{MnF}_4$ .

#### ACKNOWLEDGMENTS

This work was supported by the National Key Research and Development Program of China (Grant No. 2021YFA1601004) and the National Natural Science Foundation of China (NSFC) (Grant Nos. 11874223 and 51871121). We also acknowledge the National Supercomputer Center in Tianjin [TianHe-1(A)] and the Supercomputing Center of Nankai University (NKSC) for the computational resources and technical support.

#### AUTHOR DECLARATIONS

##### Conflict of Interest

The authors have no conflicts to disclose.

##### Author Contributions

**Baojuan Xin:** Data curation (lead); Formal analysis (lead); Methodology (equal); Writing – original draft (lead). **Kaixin Zou:** Data curation (supporting); Formal analysis (equal); Writing – review & editing (supporting). **Dayong Liu:** Formal analysis (equal); Writing – review & editing (supporting). **Shanchuan Liang:** Formal analysis (supporting); Writing – review & editing (supporting). **Hong Dong:** Formal analysis (supporting); Writing – review & editing (supporting). **Feng Lu:** Conceptualization (lead); Formal analysis (equal); Funding acquisition (lead); Methodology (equal); Supervision (equal); Writing – review & editing (supporting). **Cheng Gong:** Formal analysis (supporting); Writing – review & editing (supporting). **Feng Luo:** Formal analysis (supporting); Funding acquisition (lead); Writing – review & editing (supporting). **Wei-Hua Wang:** Conceptualization (lead); Formal analysis (equal); Funding acquisition (lead); Methodology (equal); Supervision (lead); Writing – review & editing (lead).

#### DATA AVAILABILITY

The data that support the findings of this study are available within the article and its [supplementary material](#).

#### REFERENCES

- 1K. S. Novoselov, A. K. Geim, S. V. Morozov, D. Jiang, Y. Zhang, S. V. Dubonos, I. V. Grigorieva, and A. A. Firsov, “Electric field effect in atomically thin carbon films,” *Science* **306**, 666 (2004).
- 2S. V. Morozov, K. S. Novoselov, M. I. Katsnelson, F. Schedin, D. C. Elias, J. A. Jaszczak, and A. K. Geim, “Giant intrinsic carrier mobilities in graphene and its bilayer,” *Phys. Rev. Lett.* **100**, 016602 (2008).
- 3J. Ingla-Aynés, M. H. D. Guimarães, R. J. Meijerink, P. J. Zomer, and B. J. van Wees, “24- $\mu\text{m}$  spin relaxation length in boron nitride encapsulated bilayer graphene,” *Phys. Rev. B* **92**, 201410(R) (2015).
- 4T. Fang, A. Konar, H. Xing, and D. Jena, “Carrier statistics and quantum capacitance of graphene sheets and ribbons,” *Appl. Phys. Lett.* **91**, 092109 (2007).
- 5A. H. Castro Neto, F. Guinea, N. M. R. Peres, K. S. Novoselov, and A. K. Geim, “The electronic properties of graphene,” *Rev. Mod. Phys.* **81**, 109 (2009).
- 6Y. Liu, C. Zeng, J. Zhong, J. Ding, Z. M. Wang, and Z. Liu, “Spintronics in two-dimensional materials,” *Nano Micro Lett.* **12**, 93 (2020).
- 7M. Gmitra, S. Konschuh, C. Ertler, C. Ambrosch-Draxl, and J. Fabian, “Band-structure topologies of graphene: Spin-orbit coupling effects from first principles,” *Phys. Rev. B* **80**, 235431 (2009).
- 8X. Xu, C. Liu, Z. Sun, T. Cao, Z. Zhang, E. Wang, Z. Liu, and K. Liu, “Interfacial engineering in graphene bandgap,” *Chem. Soc. Rev.* **47**, 3059 (2018).
- 9Z. H. Ni, T. Yu, Y. H. Lu, Y. Y. Wang, Y. P. Feng, and Z. X. Shen, “Uniaxial strain on graphene: Raman spectroscopy study and band-gap opening,” *ACS Nano* **2**, 2301 (2008).
- 10B. Lim, X. Y. Cui, and S. P. Ringer, “Strain-mediated bandgap engineering of straight and bent semiconductor nanowires,” *Phys. Chem. Chem. Phys.* **23**, 5407 (2021).
- 11D. Soriano, N. Leconte, P. Ordejon, J. C. Charlier, J. J. Palacios, and S. Roche, “Magnetoresistance and magnetic ordering fingerprints in hydrogenated graphene,” *Phys. Rev. Lett.* **107**, 016602 (2011).

- <sup>12</sup>L. F. Huang, M. Y. Ni, G. R. Zhang, W. H. Zhou, Y. G. Li, X. H. Zheng, and Z. Zeng, "Modulation of the thermodynamic, kinetic, and magnetic properties of the hydrogen monomer on graphene by charge doping," *J. Chem. Phys.* **135**, 064705 (2011).
- <sup>13</sup>S. J. Gong, C. Gong, Y. Y. Sun, W. Y. Tong, C. G. Duan, J. H. Chu, and X. Zhang, "Electrically induced 2D half-metallic antiferromagnets and spin field effect transistors," *Proc. Natl. Acad. Sci. U.S.A.* **115**, 8511 (2018).
- <sup>14</sup>W. Li, C. Guo, X. Xin, X. Shi, and Y. Zhao, "Tunable magnetic spin ordering in MoN<sub>2</sub> monolayer by structural deformation," *Appl. Surf. Sci.* **487**, 519 (2019).
- <sup>15</sup>X. Xin, C. Guo, R. Pang, M. Zhang, X. Shi, X. Yang, and Y. Zhao, "Theoretical and experimental studies of spin polarized carbon doped Bi<sub>2</sub>Se<sub>3</sub>," *Appl. Phys. Lett.* **115**, 042401 (2019).
- <sup>16</sup>X. Ding, X. Cui, A. Sohail, P. P. Murmu, J. Kennedy, N. Bao, J. Ding, R. Liu, M. Peng, L. Wang, X. Chu, A. Vinu, S. P. Ringer, and J. Yi, "Defects engineering induced ultrahigh magnetization in rare earth element Nd-doped MoS<sub>2</sub>," *Adv. Quantum Technol.* **4**, 2000093 (2021).
- <sup>17</sup>Y. Zhou and X. Zheng, "Generating pure spin current with spin-dependent Seebeck effect in ferromagnetic zigzag graphene nanoribbons," *J. Phys.: Condens. Matter* **31**, 315301 (2019).
- <sup>18</sup>H. Henck, Z. Ben Aziza, D. Pierucci, F. Laourine, F. Reale, P. Palczynski, J. Chaste, M. G. Silly, F. Bertran, P. Le Fèvre, E. Lhuillier, T. Wakamura, C. Mattevi, J. E. Rault, M. Calandra, and A. Ouerghi, "Electronic band structure of two-dimensional WS<sub>2</sub>/graphene van der Waals heterostructures," *Phys. Rev. B* **97**, 155421 (2018).
- <sup>19</sup>D. Kang, Z.-W. Zuo, S. Zhang, Z. Wang, and L. Zhang, "Stacking order driving bandgap and conductance of graphene/C<sub>3</sub>N (C<sub>3</sub>N) van der Waals heterostructures," *Appl. Phys. Lett.* **116**, 153103 (2020).
- <sup>20</sup>R. Li, W. Sun, C. Zhan, P. R. C. Kent, and D.-E. Jiang, "Interfacial and electronic properties of heterostructures of MXene and graphene," *Phys. Rev. B* **99**, 085429 (2019).
- <sup>21</sup>X. Shao, K. Wang, R. Pang, and X. Shi, "Lithium intercalation in graphene/MoS<sub>2</sub> composites: First-principles insights," *J. Phys. Chem. C* **119**, 25860 (2015).
- <sup>22</sup>H. Guo, Y. Yin, H. Niu, J. Robertson, Z. Zhang, and Y. Guo, "Tunable contacts and device performances in graphene/group-III monochalcogenides MX (M = In, Ga; X = S, Se) van der Waals heterostructures," *J. Appl. Phys.* **130**, 144303 (2021).
- <sup>23</sup>Y. Guo and J. Robertson, "Band engineering in transition metal dichalcogenides: Stacked versus lateral heterostructures," *Appl. Phys. Lett.* **108**, 233104 (2016).
- <sup>24</sup>R. Zhang, G. Hao, X. Ye, W. Zhang, and H. Li, "Tunable Schottky contact in the graphene/WS<sub>2</sub>(1-x)O<sub>2x</sub> heterostructure by asymmetric O doping," *J. Appl. Phys.* **129**, 174302 (2021).
- <sup>25</sup>J. Zhang, B. Zhao, T. Zhou, Y. Xue, C. Ma, and Z. Yang, "Strong magnetization and Chern insulators in compressed graphene/CrI<sub>3</sub> van der Waals heterostructures," *Phys. Rev. B* **97**, 085401 (2018).
- <sup>26</sup>S. K. Behera, M. Bora, S. S. Paul Chowdhury, and P. Deb, "Proximity effects in graphene and ferromagnetic CrBr<sub>3</sub> van der Waals heterostructures," *Phys. Chem. Chem. Phys.* **21**, 25788 (2019).
- <sup>27</sup>Z. Tu, T. Zhou, T. Ersevım, H. S. Arachchige, A. T. Hanbicki, A. L. Friedman, D. Mandrus, M. Ouyang, I. Žutić, and C. Gong, "Spin-orbit coupling proximity effect in MoS<sub>2</sub>/Fe<sub>3</sub>GeTe<sub>2</sub> heterostructures," *Appl. Phys. Lett.* **120**, 043102 (2022).
- <sup>28</sup>X. Tao, L. Zhang, X. Zheng, H. Hao, X. Wang, L. Song, Z. Zeng, and H. Guo, "h-BN/graphene van der Waals vertical heterostructure: A fully spin-polarized photocurrent generator," *Nanoscale* **10**, 174 (2018).
- <sup>29</sup>K. Zollner and J. Fabian, "Engineering proximity exchange by twisting: Reversal of ferromagnetic and emergence of antiferromagnetic Dirac bands in graphene/Cr<sub>2</sub>Ge<sub>2</sub>Te<sub>6</sub>," *Phys. Rev. Lett.* **128**, 106401 (2022).
- <sup>30</sup>W. Mi, H. Yang, Y. Cheng, G. Chen, and H. Bai, "Magnetic and electronic properties of Fe<sub>3</sub>O<sub>4</sub>/graphene heterostructures: First principles perspective," *J. Appl. Phys.* **113**, 083711 (2013).
- <sup>31</sup>B. Pan, J. Xiao, J. Li, P. Liu, C. Wang, and G. Yang, "Carbyne with finite length: The one-dimensional sp carbon," *Sci. Adv.* **1**, e1500857 (2015).
- <sup>32</sup>X. Li, H. Lv, J. Dai, L. Ma, X. C. Zeng, X. Wu, and J. Yang, "Half-metallicity in one-dimensional metal trihydride molecular nanowires," *J. Am. Chem. Soc.* **139**, 6290 (2017).
- <sup>33</sup>T. Debnath, B. Debnath, and R. K. Lake, "Thermal conductivity of the quasi-one-dimensional materials TaSe<sub>3</sub> and ZrTe<sub>3</sub>," *Phys. Rev. Mater.* **5**, 034010 (2021).
- <sup>34</sup>F. Lu, J. Cui, P. Liu, M. Lin, Y. Cheng, H. Liu, W. Wang, K. Cho, and W.-H. Wang, "High-throughput identification of one-dimensional atomic wires and first principles calculations of their electronic states," *Chin. Phys. B* **30**, 057304 (2021).
- <sup>35</sup>Y. Liu, Y. Huang, and X. Duan, "Van der Waals integration before and beyond two-dimensional materials," *Nature* **567**, 323 (2019).
- <sup>36</sup>Z. Zhang, P. Lin, Q. Liao, Z. Kang, H. Si, and Y. Zhang, "Graphene-based mixed-dimensional van der Waals heterostructures for advanced optoelectronics," *Adv. Mater.* **31**, 1806411 (2019).
- <sup>37</sup>C. Liu, H. Hong, Q. Wang, P. Liu, Y. Zuo, J. Liang, Y. Cheng, X. Zhou, J. Wang, Y. Zhao, J. Xiong, B. Xiang, J. Zhang, and K. Liu, "Strong-coupled hybrid structure of carbon nanotube and MoS<sub>2</sub> monolayer with ultrafast interfacial charge transfer," *Nanoscale* **11**, 17195 (2019).
- <sup>38</sup>Y. Zhang, J. Guo, Y. Xu, W. Huang, C. Li, L. Gao, L. Wu, Z. Shi, C. Ma, Y. Ge, X. Zhang, and H. Zhang, "Synthesis and optoelectronics of mixed-dimensional Bi/Te binary heterostructures," *Nanoscale Horiz.* **5**, 847 (2020).
- <sup>39</sup>D. Jariwala, T. J. Marks, and M. C. Hersam, "Mixed-dimensional van der Waals heterostructures," *Nat. Mater.* **16**, 170 (2017).
- <sup>40</sup>J. Zhang, L. Cong, K. Zhang, X. Jin, X. Li, Y. Wei, Q. Li, K. Jiang, Y. Luo, and S. Fan, "Mixed-dimensional vertical point p-n junctions," *ACS Nano* **14**, 3181 (2020).
- <sup>41</sup>G. Kresse and J. Furthmüller, "Efficient iterative schemes for *ab initio* total-energy calculations using a plane-wave basis set," *Phys. Rev. B* **54**, 11169 (1996).
- <sup>42</sup>J. P. Perdew, K. Burke, and M. Ernzerhof, "Generalized gradient approximation made simple," *Phys. Rev. Lett.* **77**, 3865 (1996).
- <sup>43</sup>S. Grimme, "Semiempirical GGA-type density functional constructed with a long-range dispersion correction," *J. Comput. Chem.* **27**, 1787 (2006).
- <sup>44</sup>S. Xu, F. Jia, X. Cheng, and W. Ren, "Predicting intrinsic antiferromagnetic and ferroelastic MnF<sub>4</sub> monolayer with controllable magnetization," *J. Mater. Chem. C* **9**, 17152 (2021).
- <sup>45</sup>E. Sanville, S. D. Kenny, R. Smith, and G. Henkelman, "Improved grid-based algorithm for Bader charge allocation," *J. Comput. Chem.* **28**, 899 (2007).
- <sup>46</sup>C. Liu, Y. Han, Q. Li, Y. Ma, Y. Ma, and C. Gao, "Size-dependent phase transition of graphite to superhard graphite under high pressure at room temperature," *J. Appl. Phys.* **112**, 103707 (2012).
- <sup>47</sup>Z. Chi, X. Chen, F. Yen, F. Peng, Y. Zhou, J. Zhu, Y. Zhang, X. Liu, C. Lin, S. Chu, Y. Li, J. Zhao, T. Kagayama, Y. Ma, and Z. Yang, "Superconductivity in pristine 2H<sub>g</sub>-MoS<sub>2</sub> at ultrahigh pressure," *Phys. Rev. Lett.* **120**, 037002 (2018).
- <sup>48</sup>L. Zhang, Y. Tang, A. R. Khan, M. M. Hasan, P. Wang, H. Yan, T. Yildirim, J. F. Torres, G. P. Neupane, Y. Zhang, Q. Li, and Y. Lu, "2D materials and heterostructures at extreme pressure," *Adv. Sci.* **7**, 2002697 (2020).
- <sup>49</sup>Y. Cao, V. Fatemi, A. Demir, S. Fang, S. L. Tomarken, J. Y. Luo, J. D. Sanchez-Yamagishi, K. Watanabe, T. Taniguchi, E. Kaxiras, R. C. Ashoori, and P. Jarillo-Herrero, "Correlated insulator behaviour at half-filling in magic-angle graphene superlattices," *Nature* **556**, 80 (2018).
- <sup>50</sup>Y. Cao, V. Fatemi, S. Fang, K. Watanabe, T. Taniguchi, E. Kaxiras, and P. Jarillo-Herrero, "Unconventional superconductivity in magic-angle graphene superlattices," *Nature* **556**, 43 (2018).
- <sup>51</sup>D. M. Kennes, L. Xian, M. Claassen, and A. Rubio, "One-dimensional flat bands in twisted bilayer germanium selenide," *Nat. Commun.* **11**, 1124 (2020).
- <sup>52</sup>J. Wang, M. Ge, R. Ma, Y. Sun, L. Cheng, R. Wang, M. Guo, and J. Zhang, "Twist angle dependent electronic properties in 2D graphene/MoS<sub>2</sub> vdW heterostructures," *J. Appl. Phys.* **131**, 034301 (2022).
- <sup>53</sup>K. Liu, L. Zhang, T. Cao, C. Jin, D. Qiu, Q. Zhou, A. Zettl, P. Yang, S. G. Louie, and F. Wang, "Evolution of interlayer coupling in twisted molybdenum disulfide bilayers," *Nat. Commun.* **5**, 4966 (2014).

- <sup>54</sup>X. Gao, Y. Shen, Y. Ma, S. Wu, and Z. Zhou, "Graphene/g-GeC bilayer heterostructure: Modulated electronic properties and interface contact via external vertical strains and electric fields," *Carbon* **146**, 337 (2019).
- <sup>55</sup>C. X. Xia, B. Xue, T. X. Wang, Y. T. Peng, and Y. Jia, "Interlayer coupling effects on Schottky barrier in the arsenene-graphene van der Waals heterostructure," *Appl. Phys. Lett.* **107**, 193107 (2015).
- <sup>56</sup>J. Bardeen, "Surface states and rectification at a metal semi-conductor contact," *Phys. Rev.* **71**, 717 (1947).
- <sup>57</sup>R. Zacharia, H. Ulbricht, and T. Hertel, "Interlayer cohesive energy of graphite from thermal desorption of polyaromatic hydrocarbons," *Phys. Rev. B* **69**, 155406 (2004).
- <sup>58</sup>A. Azizi, S. Eichfeld, G. Geschwind, K. Zhang, B. Jiang, D. Mukherjee, L. Hossain, A. F. Piasecki, B. Kabius, J. A. Robinson, and N. Alem, "Freestanding van der Waals heterostructures of graphene and transition metal dichalcogenides," *ACS Nano* **9**, 4882 (2015).
- <sup>59</sup>C. Tang, Z. Zhang, S. Lai, Q. Tan, and W.-B. Gao, "Magnetic proximity effect in graphene/CrBr<sub>3</sub> van der Waals heterostructures," *Adv. Mater.* **32**, 1908498 (2020).